

Isospin splitting of nucleon effective mass from giant resonances in ^{208}Pb

Zhen Zhang¹ and Lie-Wen Chen^{*1,2}

¹*Department of Physics and Astronomy and Shanghai Key Laboratory for Particle Physics and Cosmology, Shanghai Jiao Tong University, Shanghai 200240, China*

²*Center of Theoretical Nuclear Physics, National Laboratory of Heavy Ion Accelerator, Lanzhou 730000, China*
(Dated: February 22, 2019)

Based on mean field calculations with Skyrme interactions, we extract a constraint on the isovector effective mass in nuclear matter at saturation density ρ_0 , i.e., $m_v^*(\rho_0) = (0.77 \pm 0.03)m$ by combining the experimental data of the centroid energy of the isovector giant dipole resonance (IVGDR) and the electric dipole polarizability in ^{208}Pb . Meanwhile, the isoscalar effective mass at ρ_0 is determined to be $m_s^*(\rho_0) = (0.91 \pm 0.05)m$ by analyzing the measured excitation energy of the isoscalar giant quadrupole resonance (ISGQR) in ^{208}Pb . From the constrained $m_s^*(\rho_0)$ and $m_v^*(\rho_0)$, we obtain the isospin splitting of nucleon effective mass in asymmetric nuclear matter of isospin asymmetry δ at ρ_0 as $(m_n^*(\rho_0, \delta) - m_p^*(\rho_0, \delta))/m = \Delta m_1^*(\rho_0)\delta + O(\delta^3)$ with the linear isospin splitting coefficient $\Delta m_1^*(\rho_0) = 0.33 \pm 0.16$. Furthermore, the constraints on $m_v^*(\rho)$, $m_s^*(\rho)$ and $\Delta m_1^*(\rho)$ at other densities are obtained from the similar analyses and we find that the $\Delta m_1^*(\rho)$ increases with the density.

PACS numbers: 21.65.-f, 24.30.Cz, 21.60.Jz, 21.30.Fe

I. INTRODUCTION

Nucleon effective mass, which is usually introduced to characterize the dynamical properties for the propagation of (quasi)nucleons in nuclear medium, is of fundamental importance in nuclear many-body physics [1–3]. While there exist several different kinds of nucleon effective masses in non-relativistic and relativistic approaches [4–7], we shall focus in this work on the total nucleon effective mass used typically in the non-relativistic approach, which measures the momentum dependence (or equivalently energy dependence by assuming an on-shell dispersion relation) of the nucleon single-particle potential. In isospin asymmetric nuclear matter, neutrons and protons may feel different single-particle potentials which can then lead to the isospin splitting of nucleon effective mass, i.e., $m_{n-p}^* \equiv (m_n^* - m_p^*)/m$. The isospin splitting of nucleon effective mass may have a profound impact on various physical phenomena and quantities in nuclear physics, astrophysics and cosmology [8, 9], such as the properties of mirror nuclei [10], transport properties of asymmetric nuclear matter [11–20], neutrino emission in neutron stars [21], and the primordial nucleosynthesis in the early universe [22].

Theoretical studies based on either microscopic many-body theories or phenomenological approaches have thus far given widely divergent predictions on m_{n-p}^* . For example, non-relativistic Brueckner-Hartree-Fock and relativistic Dirac-Brueckner-Hartree-Fock calculations indicate $m_{n-p}^* > 0$ [23–25] in neutron-rich matter, while relativistic mean field, Skyrme-Hartree-Fock (SHF) and Gogny-Hartree-Fock models predict either $m_{n-p}^* > 0$ or $m_{n-p}^* < 0$ [6, 26–32], depending on the interactions. During the last several years, significant progress has been

made in determining the isospin splitting of nucleon effective mass by analyzing experimental data [9]. However, there is still no quantitatively and even qualitatively consensus on the behavior of m_{n-p}^* in asymmetric nuclear matter. For example, while the optical model analyses of nucleon-nucleus scattering data [33, 34] favor $m_{n-p}^* > 0$ in neutron-rich matter at ρ_0 , the transport model analysis on the double n/p ratio in heavy ion collisions seems to suggest the opposite conclusion [35] (but see Ref. [36]).

Nuclear giant resonances provide an important approach to determine nucleon effective mass. It has been well established that the excitation energy E_x of the isoscalar giant quadrupole resonance (ISGQR) in finite nuclei is related to the isoscalar effective mass $m_s^*(\rho)$ (nucleon effective mass in symmetric nuclear matter) at ρ_0 , i.e., $m_{s,0}^*$ (see, e.g., Refs. [37–40]). A value of $m_{s,0}^* \sim 0.8m$ has been estimated by analyzing experimental data for ISGQR excitation energy in early studies [38], and more recent microscopic random phase approximation (RPA) calculations suggest that the ISGQR in heavy nuclei favors $m_{s,0}^* \sim 0.9m$ [39–41]. Moreover, within the RPA approach using Skyrme interactions, the isovector effective mass $m_v^*(\rho)$ (i.e., neutron (proton) effective mass in pure proton (neutron) matter) at ρ_0 , i.e., $m_{v,0}^*$, is directly related to the enhancement factor κ of the energy weighted sum rule (EWSR) m_1 in the isovector giant dipole resonance (IVGDR) [41–43]. Unfortunately, while the peak of the IVGDR strength function has been well located by photoabsorption measurements [44], neither m_1 nor κ has been accurately determined. Therefore, the $m_{v,0}^*$ has so far not yet been properly constrained.

Thanks to the recent high resolution measurement for the electric dipole polarizability α_D in ^{208}Pb at the Research Center for Nuclear Physics (RCNP) [45], in this work, we deduce the m_1 of the IVGDR in ^{208}Pb from the experimental value of the IVGDR centroid energy [44]. Using the RPA calculations with a number of representative Skyrme interactions, we then extract relatively ac-

*Corresponding author (email: lwchen@sjtu.edu.cn)

curate constraints on m_s^* and m_v^* from the ISGQR excitation energy and the m_1 of the IVGDR in ^{208}Pb , respectively. Within the SHF model, since the m_{n-p}^* is completely determined by the m_s^* and m_v^* , we thus further obtain constraints on the m_{n-p}^* . For the first time, our results indicate that the data on the giant resonances in ^{208}Pb favor $m_{n-p}^* > 0$ in neutron-rich matter, which would be very helpful to address the issue on the isospin splitting of nucleon effective mass.

II. MODEL AND METHOD

A. Nucleon effective mass in Skyrme-Hartree-Fock approach

In non-relativistic approaches, the effective mass m_q^* of a nucleon q (n or p) in asymmetric nuclear matter with density ρ and isospin asymmetry $\delta = (\rho_n - \rho_p)/(\rho_p + \rho_n)$ can be calculated as [1]

$$\frac{m_q^*(\rho, \delta)}{m_q} = \left[1 + \frac{m_q}{k} \frac{dU_q(k, \epsilon_q(k, \rho, \delta), \rho, \delta)}{dk} \Big|_{k_F^q} \right]^{-1}, \quad (1)$$

where m_q represents the mass of neutrons or protons in free-space ($m_q = m$ is assumed in this work), k_F^q is the neutron/proton Fermi momentum, U_q is the single-nucleon potential, and ϵ_q is the nucleon single-particle energy satisfying the following dispersion relation

$$\epsilon_q(k, \rho, \delta) = \frac{k^2}{2m_q} + U_q(k, \epsilon_q(k), \rho, \delta). \quad (2)$$

In this work, we use the standard Skyrme interaction with a zero-range and velocity-dependent form as [43]

$$\begin{aligned} V_{12}(\mathbf{R}, \mathbf{r}) = & t_0(1 + x_0 P_\sigma) \delta(\mathbf{r}) \\ & + \frac{1}{6} t_3(1 + x_3 P_\sigma) \rho^\sigma(\mathbf{R}) \delta(\mathbf{r}) \\ & + \frac{1}{2} t_1(1 + x_1 P_\sigma) (\mathbf{K}'^2 \delta(\mathbf{r}) + \delta(\mathbf{r}) \mathbf{K}^2) \\ & + t_2(1 + x_2 P_\sigma) \mathbf{K}' \cdot \delta(\mathbf{r}) \mathbf{K} \\ & + i W_0(\sigma_1 + \sigma_2) \cdot [\mathbf{K}' \times \delta(\mathbf{r}) \mathbf{K}], \end{aligned} \quad (3)$$

with $\mathbf{r} = \mathbf{r}_1 - \mathbf{r}_2$ and $\mathbf{R} = (\mathbf{r}_1 + \mathbf{r}_2)/2$. In the above expression, the relative momentum operators $\mathbf{K} = (\nabla_1 - \nabla_2)/2i$ and $\mathbf{K}' = -(\nabla_1 - \nabla_2)/2i$ act on the wave function on the right and left, respectively. The quantities P_σ and σ_i denote, respectively, the spin exchange operator and Pauli spin matrices. In the following, several Skyrme interactions with nonstandard spin-orbit term [46] are also employed, but we notice that the spin-orbit term is irrelevant to the expressions of nucleon effective mass.

Within the standard SHF approach, the nucleon effective mass in asymmetric nuclear matter with density ρ

and isospin asymmetry δ can be expressed as [43]

$$\begin{aligned} \frac{\hbar^2}{2m_q^*(\rho, \delta)} = & \frac{\hbar^2}{2m} + \frac{1}{4} t_1 \left[\left(1 + \frac{1}{2} x_1 \right) \rho - \left(\frac{1}{2} + x_1 \right) \rho_q \right] \\ & + \frac{1}{4} t_2 \left[\left(1 + \frac{1}{2} x_2 \right) \rho + \left(\frac{1}{2} + x_2 \right) \rho_q \right]. \end{aligned} \quad (4)$$

By setting $\rho_q = \rho/2$ in Eq. (4), the isoscalar effective mass can then be obtained as [43]

$$\frac{\hbar^2}{2m_s^*(\rho)} = \frac{\hbar^2}{2m} + \frac{3}{16} t_1 \rho + \frac{1}{16} t_2 (4x_2 + 5) \rho. \quad (5)$$

The isovector effective mass, which corresponds to the proton (neutron) effective mass in pure neutron (proton) matter, can be obtained with $\rho_q = 0$ in Eq. (4) as [43]

$$\frac{\hbar^2}{2m_v^*(\rho)} = \frac{\hbar^2}{2m} + \frac{1}{8} t_1 (x_1 + 2) \rho + \frac{1}{8} t_2 (x_2 + 2) \rho. \quad (6)$$

From Eqs. (4), (5) and (6), one can obtain the isospin splitting of nucleon effective mass, i.e.,

$$\begin{aligned} m_{n-p}^*(\rho, \delta) & \equiv \frac{m_n^* - m_p^*}{m} = 2 \frac{m_s^*}{m} \sum_{n=1}^{\infty} \left(\frac{m_s^* - m_v^*}{m_v^*} \delta \right)^{2n-1} \\ & = \sum_{n=1}^{\infty} \Delta m_{2n-1}^*(\rho) \delta^{2n-1}, \end{aligned} \quad (7)$$

where the isospin splitting coefficients $\Delta m_{2n-1}^*(\rho)$ can be expressed as

$$\Delta m_{2n-1}^*(\rho) = 2 \frac{m_s^*}{m} \left(\frac{m_s^*}{m_v^*} - 1 \right)^{2n-1}. \quad (8)$$

The above expressions reveal that, within the SHF model, the m_{n-p}^* is completely determined by the m_s^* and m_v^* , and the sign of m_{n-p}^* in neutron-rich matter is the same as that of $m_s^* - m_v^*$.

B. Random-phase approximation and nuclear giant resonances

The random-phase approximation provides a successful microscopic approach to study giant resonance observables in finite nuclei. Within the framework of RPA theory, for a given excitation operator \hat{F}_{JM} , the reduced transition probability from RPA ground state $|\tilde{0}\rangle$ to RPA excitation state $|\nu\rangle$ is given by:

$$\begin{aligned} B(EJ : \tilde{0} \rightarrow |\nu\rangle) & = |\langle \nu | \hat{F}_J | \tilde{0} \rangle|^2 \\ & = \left| \sum_{mi} (X_{mi}^\nu + Y_{mi}^\nu) |\langle m | \hat{F}_J | i \rangle| \right|^2, \end{aligned} \quad (9)$$

where $m(i)$ denotes the unoccupied (occupied) single nucleon state; $\langle m | \hat{F}_J | i \rangle$ is the reduced matrix element of

\hat{F}_{JM} ; and X_{mi}^ν and Y_{mi}^ν are the RPA amplitudes. The strength function then can be calculated as:

$$S(E) = \sum_{\nu} |\langle \nu | \hat{F}_J | \tilde{0} \rangle|^2 \delta(E - E_{\nu}), \quad (10)$$

where E_{ν} is the energy of RPA excitation state $|\nu\rangle$. Thus the moments of strength function can be obtained as:

$$m_k = \int dE E^k S(E) = \sum_{\nu} |\langle \nu | \hat{F}_J | \tilde{0} \rangle|^2 E_{\nu}^k. \quad (11)$$

For the IVGDR and IVGQR that we are interested in here, the excitation operators are defined as:

$$\hat{F}_{1M} = \frac{N}{A} \sum_{i=1}^Z r_i Y_{1M}(\hat{r}_i) - \frac{Z}{A} \sum_{i=1}^N r_i Y_{1M}(\hat{r}_i), \quad (12)$$

$$\hat{F}_{2M} = \sum_{i=1}^A r_i^2 Y_{2M}(\hat{r}_i), \quad (13)$$

where Z , N and A are proton, neutron and mass number, respectively; r_i is the nucleon's radial coordinate; $Y_{1M}(\hat{r}_i)$ and $Y_{2M}(\hat{r}_i)$ are the corresponding spherical harmonic function.

C. Nucleon effective mass and nuclear giant resonances

It is well known that the isoscalar effective mass at saturation density, i.e., $m_{s,0}^*$, is intimately related to the excitation energy of the ISGQR in finite nuclei. In the harmonic oscillator model, the ISGQR energy is [37, 39]

$$E_x = \sqrt{\frac{2m}{m_{s,0}^*}} \hbar \omega_0, \quad (14)$$

where $\hbar \omega_0$ is the frequency of the harmonic oscillator. This semiempirical expression reveals the correlation between the ISGQR excitation energy and the isoscalar effective mass $m_{s,0}^*$, which has been also confirmed by microscopic calculations [39, 40].

Meanwhile, the isovector effective mass at saturation density $m_{v,0}^*$ is correlated with the energy weighted sum rule m_1 of the IVGDR [47], i.e.

$$m_1 = \frac{9}{4\pi} \frac{\hbar^2}{2m} \frac{NZ}{A} (1 + \kappa), \quad (15)$$

where κ is the enhancement factor reflecting the deviation from the Thomas-Reiche-Kuhn sum rule [48] (e.g., due to the exchange and momentum dependent force). Within the Skyrme-RPA approach, κ is given by [43, 47]

$$\kappa = \frac{2m}{\hbar^2} \frac{A}{4NZ} \int \rho_n(r) \rho_p(r) d^3r \cdot \left[t_1 \left(1 + \frac{x_1}{2} \right) + t_2 \left(1 + \frac{x_2}{2} \right) \right]. \quad (16)$$

Substituting Eqs. (6) and (16) into Eq. (15) leads to

$$m_1 = \frac{9}{4\pi} \frac{\hbar^2}{2m} \frac{NZ}{A} \cdot \left[1 + \frac{A}{NZ} \left(\frac{m}{m_{v,0}^*} - 1 \right) \frac{\int \rho_n(r) \rho_p(r) d^3r}{\rho_0} \right] \quad (17)$$

which suggests that the EWSR of the IVGDR is proportional to $(m_{v,0}^*/m)^{-1}$. In particular, by setting $\rho_n = \rho_p = \rho_0/2$, one then obtains the following expression [43]

$$m_1 = \frac{9}{4\pi} \frac{\hbar^2}{2m} \frac{NZ}{A} \left(\frac{m_{v,0}^*}{m} \right)^{-1}, \quad (18)$$

with the relation $m_{v,0}^*/m = 1/(1 + \kappa)$.

III. RESULTS AND DISCUSSIONS

To study the correlation between effective mass and giant resonance observables, we select 50 representative Skyrme interactions [28, 49, 50] (i.e., BSk1, BSk2, BSk5, BSk6, BSk13, Es, Gs, KDE, KDE0v1, MSk7, MSL0, MSL1, NRAPR, Rs, SAMi, SGI, SGII, SK255, SK272, SKa, SkI3, SkM, SkMP, SkM*, SkP, SkS1, SkS2, SkS3, SkS4, SkSC15, SkT7, SkT8, SkT9, SKX, SKXce, SKXm, Skxs15, Skxs20, SLy4, SLy5, SLy10, SV-K241, v070, v075, v080, v090, v105, v110, Zs, Zs*). The corresponding ISGQR excitation energies and EWSRs of the IVGDR in ^{208}Pb are calculated by using the Skyrme-RPA program by Colò. *et al* [47].

In the calculation of the ISGQR excitation energy E_x , we smear out the strength function with Lorentzian functions with a width 1 MeV. We note that varying the width has little influence on the peak energy. The obtained data-to-data relations between $10^3/E_x^2$ in ^{208}Pb and $m_{s,0}/m$ predicted by the chosen 50 Skyrme interactions are displayed in Fig. 1. Also included in Fig. 1 is the linear fit together with the corresponding Pearson correlation coefficient r . As expected from the semiempirical relation Eq. (14), one can see that a strong linear correlation exists between $1/E_x^2$ and $m_{s,0}^*/m$ with the coefficient r as large as 0.971. And the linear fit gives

$$\frac{10^3}{E_x^2} = (0.66 \pm 0.26) + (8.49 \pm 0.30) \left(\frac{m_{s,0}^*}{m} \right), \quad (19)$$

where the E_x is in MeV.

In the present work, we invoke the weighted average of experimental values for the ISGQR energy in ^{208}Pb , i.e., $E_x = 10.9 \pm 0.1$ MeV [39], which is shown as the hatched band in Fig. 1. Combining this weighted average and Eq. (19), we extract the isoscalar effective mass at saturation density as

$$\frac{m_{s,0}^*}{m} = 0.91 \pm 0.05. \quad (20)$$

Here the error is obtained from the propagation of the experimental uncertainty of E_x and parameter errors in

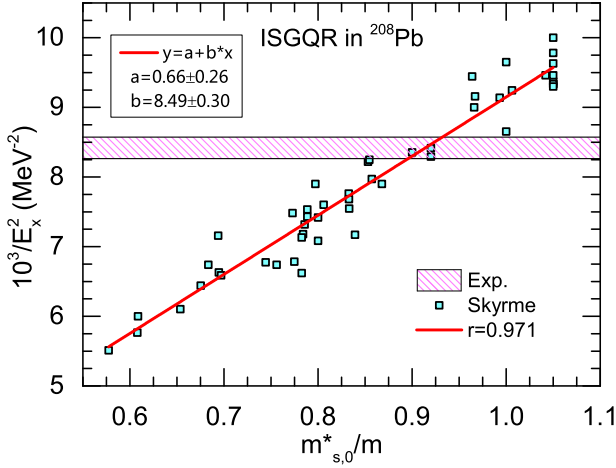


FIG. 1: (Color online) $10^3/E_x^2$ in ^{208}Pb vs $m_{s,0}^*/m$ predicted by a large number (50) of Skyrme interactions. The linear fit gives $10^3/E_x^2 = (0.66 \pm 0.26) + (8.49 \pm 0.30) (m_{s,0}^*/m)$ with the Pearson correlation coefficient being 0.971. The hatched band corresponds to the weighted averages of the experimental values for the ISGQR excitation energy in ^{208}Pb , $E_x = 10.9 \pm 0.1$ MeV [39].

the linear fit. This constraint is consistent with the result $m_{s,0}^* \approx 0.8 - 0.9m$ obtained from analyzing the ISGQR of Nd and Sm isotopes [51], and naturally confirms the empirical value of $m_{s,0}^* \sim 0.9m$ predicted by some Skyrme interactions which are obtained by fitting the experimental data of the ISGQR excitation energy in finite nuclei [40, 41]. It is also in good agreement with the result of $m_{s,0}^* \sim 0.92m$ from the extended Brueckner-Hartree-Fock calculation with realistic nucleonic forces [23].

For the IVGDR, we use the chosen 50 Skyrme interactions to evaluate the m_1 of the IVGDR in ^{208}Pb up to 130 MeV. Similarly, in Fig. 2, we plot the data-to-data relations between $10^4/m_1$ and $m_{v,0}^*/m$ as well as the linear fit and Pearson correlation coefficient r . It is clearly shown that an excellent linear correlation exists between $1/m_1$ and $m_{v,0}^*/m$, and the linear fit gives

$$\frac{10^4}{m_1} = (2.17 \pm 0.05) + (11.5 \pm 0.07) \frac{m_{v,0}^*}{m}, \quad (21)$$

where the m_1 is in $\text{MeV} \cdot \text{fm}^2$. Experimentally, the centroid energy of the IVGDR, i.e., $E_{-1} = \sqrt{m_1/m_{-1}}$, in ^{208}Pb has been well determined from photoabsorption measurements, i.e., $E_{-1} = 13.46$ MeV [44], and the inverse energy weighted sum rule m_{-1} can be obtained from the experimental value of the electric dipole polarizability measured at RCNP, i.e., $\alpha_D = 20.1 \pm 0.6 \text{ fm}^3$ [45], through the following simple relation

$$m_{-1} = \frac{9}{8\pi e^2} \alpha_D. \quad (22)$$

The experimental values of E_{-1} and m_{-1} together thus give $m_1 = 905.60 \pm 27.03 \text{ MeV} \cdot \text{fm}^2$. Therefore, one can

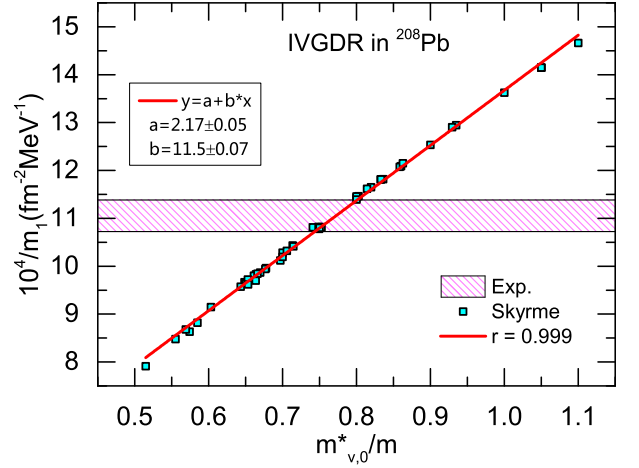


FIG. 2: (Color online) $10^4/m_1$ in ^{208}Pb vs $m_{v,0}^*/m$ predicted by a large number (50) of Skyrme interactions. The linear fit gives $10^4/m_1 = (2.17 \pm 0.05) + (11.5 \pm 0.07) m_{v,0}^*/m$ with the Pearson correlation coefficient being 0.999. The hatched band corresponds to the experimental value of the EWSR m_1 of the IVGDR in ^{208}Pb (see text for detail).

constrain isovector effective mass at saturation density using Eq. (21), and the result is

$$\frac{m_{v,0}^*}{m} = 0.77 \pm 0.03. \quad (23)$$

One can see that our constraint is rather accurate and well consistent with the empirical value, e.g., $m_{v,0}^*/m = 0.90 \pm 0.2$ from analyses of finite nuclei mass data [52]. In addition, from the well known relation $m_{v,0}^*/m = 1/(1 + \kappa)$, the value of the enhancement factor κ can be deduced as $\kappa = 0.30 \pm 0.05$, which is a little higher than $\kappa = 0.22 \pm 0.04$ reported in Ref. [53].

From the constraints on $m_{s,0}^*$ and $m_{v,0}^*$, one can then obtain the isospin splitting $m_{n-p}^*(\rho_0)$ according to Eq. (8). In particular, we obtain the first-order (linear) isospin splitting coefficient $\Delta m_1^*(\rho)$ at ρ_0 as

$$\Delta m_1^*(\rho_0) = 0.33 \pm 0.16, \quad (24)$$

which is in very good agreement with the constraint $\Delta m_1^*(\rho_0) = 0.32 \pm 0.15$ obtained in Ref. [33] and the more recent constraint $\Delta m_1^*(\rho_0) = 0.41 \pm 0.15$ extracted in Ref. [34] from the global optical model analysis of nucleon-nucleus scattering data. The present result is also consistent with the $\Delta m_1^*(\rho_0) = 0.27$ obtained by analyzing various constraints on the magnitude and density slope of the symmetry energy at ρ_0 [54]. The positive value of $\Delta m_1^*(\rho_0)$ further agrees with the microscopic Brueckner calculations with realistic nuclear forces [23–25]. In addition, it is interesting to see that the higher-order isospin splitting coefficients are rather small and can be neglected safely. For example, the third-order isospin splitting coefficient $\Delta m_3^*(\rho_0)$ is found to be 0.01 ± 0.01 .

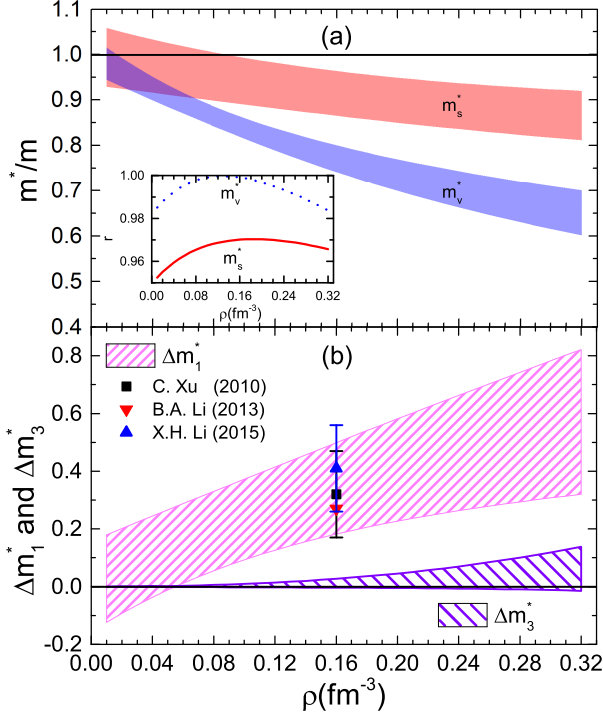


FIG. 3: (Color online) Panel (a): Constraints on the density dependence of the isoscalar and isovector effective mass, m_s^* and m_v^* , extracted from the ISGQR and IVGDR in ^{208}Pb , respectively. The inset shows the corresponding Pearson correlation coefficient r as a function of density. Panel (b): Constraint on the density dependence of the isospin splitting coefficients $\Delta m_1^*(\rho)$ and $\Delta m_3^*(\rho)$ obtained in this work. The $\Delta m_1^*(\rho)$ constraints obtained in Refs. [33, 34, 54] are also included for comparison.

The above analyses are only made at saturation density ρ_0 and it is also interesting to see the constraints on $m_s^*(\rho)$, $m_v^*(\rho)$ and $m_{n-p}^*(\rho)$ at other densities. Similar analyses indicate that the strong linear correlation also exists between $1/E_x^2$ and $m_s^*(\rho)/m$ as well as between $1/m_1$ and $m_v^*(\rho)/m$ at other densities ρ . Shown in Fig. 3 (a) are the constraints on the $m_s^*(\rho)/m$ and $m_v^*(\rho)/m$ as functions of density extracted from the ISGQR and IVGDR in ^{208}Pb , respectively. The inset of Fig. 3 (a) shows the density dependence of the corresponding Pearson correlation coefficient r for $1/E_x^2$ vs $m_s^*(\rho)/m$ as well as $1/m_1$ vs $m_v^*(\rho)/m$. The corresponding constraints on the isospin splitting coefficients $\Delta m_1^*(\rho)$ and $\Delta m_3^*(\rho)$ as functions of density are shown in Fig. 3 (b). Also included in Fig. 3 (b) are the $\Delta m_1^*(\rho)$ constraints obtained in Refs. [33, 34, 54] as discussed earlier. Indeed, one can see that all the r values in the inset of Fig. 3 (a) are larger than 0.95 for $0 < \rho < 0.32 \text{ fm}^{-3}$ that we are considering here, indicating the strong linear correlation. Particularly, the strongest correlation appears at $\rho \approx 0.19 \text{ fm}^{-3}$ (with $r = 0.97035$) for $1/E_x^2$ vs $m_s^*(\rho)/m$ while at $\rho \approx 0.13 \text{ fm}^{-3}$ (with $r = 0.99961$) for $1/m_1$ vs $m_v^*(\rho)/m$. It is seen that the $m_s^*(\rho)/m$ is generally larger

than $m_v^*(\rho)/m$ and both $m_s^*(\rho)/m$ and $m_v^*(\rho)/m$ decrease with density but the latter exhibits a stronger density dependence, which leads to the isospin splitting coefficients $\Delta m_1^*(\rho)$ and $\Delta m_3^*(\rho)$ increases with density as observed in Fig. 3 (b). It is interesting to see that the third-order isospin splitting coefficient $\Delta m_3^*(\rho)$ is very small (about 0.05 even at $\rho = 0.32 \text{ fm}^{-3}$) and can be approximately negligible. The stronger isospin splitting of nucleon effective mass at higher densities may have implications on the isospin effects in heavy ion collisions and neutrino emission in neutron stars as mentioned earlier, and these are deserved further explorations in future.

IV. CONCLUSIONS

Based on mean field calculations with Skyrme interactions, we have demonstrated that the isoscalar and isovector effective masses at saturation density, i.e., $m_{s,0}^*$ and $m_{v,0}^*$, can be well constrained by the ISGQR excitation energy E_x and the EWSR m_1 of the IVGDR in ^{208}Pb , respectively. In particular, invoking the experimental data for E_x in ^{208}Pb , we have obtained the constraint $m_{s,0}^* = 0.91 \pm 0.05m$. Meanwhile, combining the experimental IVGDR centroid energy and the electric dipole polarizability α_D in ^{208}Pb , we have deduced a value of $m_1 = 905.60 \pm 27.03 \text{ MeV} \cdot \text{fm}^2$, and further extracted a value of $m_{v,0}^* = 0.77 \pm 0.03m$. From the extracted $m_{s,0}^*$ and $m_{v,0}^*$, we have obtained a constraint on the first-order (linear) isospin splitting coefficient of nucleon effective mass, i.e., $\Delta m_1^*(\rho_0) = 0.33 \pm 0.16$, which is in good agreement with the constraints extracted from global nucleon optical potentials constrained by world data on nucleon-nucleus scattering [33, 34] and is also consistent with the value obtained by analyzing the constraints on the symmetry energy [54].

Furthermore, we have constrained the isoscalar and isovector effective masses as well as the isospin splitting of nucleon effective mass at other densities by the similar analyses of the giant resonances in ^{208}Pb . Our results indicate that the isospin splitting of nucleon effective mass increases with the density, and the third-order or higher-order isospin splitting coefficients are negligibly small.

Our present work reveals for the first time that the data on the giant resonances in ^{208}Pb favor $m_n^* > m_p^*$ in neutron-rich matter, which sheds a light upon understanding the isospin splitting of nucleon effective mass in asymmetric nuclear mass. The results in the present work have been obtained within mean field calculations with Skyrme interactions. It will be interesting to see how our results change if different interactions are used and/or effects beyond mean field approximation are included.

Acknowledgments

We are grateful to Li-Gang Cao for helpful discussions on the Skyrme-RPA code. This work was supported in part by the Major State Basic Research Development Program (973 Program) in China under Contract Nos. 2013CB834405 and 2015CB856904, the NNSF

of China under Grant Nos. 11275125 and 11135011, the “Shu Guang” project supported by Shanghai Municipal Education Commission and Shanghai Education Development Foundation, the Program for Professor of Special Appointment (Eastern Scholar) at Shanghai Institutions of Higher Learning, and the Science and Technology Commission of Shanghai Municipality (11DZ2260700).

-
- [1] J.P. Jeukenne, A. Lejeune, and C. Mahaux, *Phys. Rep.* **25**, 83 (1976).
 - [2] O. Sjöberg, *Nucl. Phys.* **A265**, 511 (1976).
 - [3] J.W. Negele and K. Yazaki, *Phys. Rev. Lett.* **62**, 71 (1981).
 - [4] C. Mahaux, P.F. Bortignon, R.A. Broglia, and C.H. Dasso, *Phys. Rep.* **120**, 1 (1985).
 - [5] M. Jaminon and C. Mahaux, *Phys. Rev. C* **40**, 354 (1989).
 - [6] L.W. Chen, C.M. Ko, and B.A. Li, *Phys. Rev. C* **76**, 054316 (2007).
 - [7] B.A. Li, L.W. Chen, and C.M. Ko, *Phys. Rep.* **464**, 113 (2008).
 - [8] Ulf-G. Meißner, A.M. Rakhimov, A. Wirzba, and U.T. Yakhshiev, *Eur. Phys. J. A* **31**, 357 (2007); *ibid.* **32**, 299 (2007); *ibid.* **36**, 37 (2008).
 - [9] B.A. Li and L.W. Chen, *Mod. Phys. Lett.* **A30**, 1530010 (2015).
 - [10] J.A. Nolen and J.P. Schiffer, *Ann. Rev. Nucl. Part. Sci.* **19**, 471 (1969).
 - [11] B.A. Li, C.B. Das, S. Das Gupta, and C. Gale, *Phys. Rev. C* **69**, 011603 (2004); *Nucl. Phys.* **A735**, 563 (2004).
 - [12] B.A. Li and L.W. Chen, *Phys. Rev. C* **72**, 064611 (2005).
 - [13] J. Rizzo, M. Colonna, and M. Di Toro, *Phys. Rev. C* **72**, 064609 (2005).
 - [14] V. Giordano et al., *Phys. Rev. C* **81**, 044611 (2010).
 - [15] Z.Q. Feng, *Nucl. Phys.* **A878**, 3 (2012); *Phys. Lett.* **B707**, 83 (2012).
 - [16] Y. Zhang, M.B. Tsang, Z. Li, and H. Liu, *Phys. Lett.* **B732**, 186 (2014).
 - [17] W.J. Xie and F.S. Zhang, *Phys. Lett.* **B735**, 250 (2014).
 - [18] B. Behera, T.R. Routray, and S.K. Tripathy, *J. Phys. G* **38**, 115104 (2011).
 - [19] J. Xu, L.W. Chen, and B.A. Li, *Phys. Rev. C* **91**, 014611 (2015).
 - [20] J. Xu, *Phys. Rev. C* **91**, 037601 (2015).
 - [21] M. Baldo, G. F. Burgio, H.-J. Schulze, and G. Taranto, *Phys. Rev. C* **89**, 048801 (2014).
 - [22] G. Steigman, *Int. J. Mod. Phys. E* **15**, 1 (2006).
 - [23] W. Zuo, I. Bombaci, and U. Lombardo, *Phys. Rev. C* **60**, 024605 (1999); W. Zuo, L.G. Cao, B.A. Li, U. Lombardo, and C. W. Shen, *Phys. Rev. C* **72**, 014005 (2005).
 - [24] Z.Y. Ma, J. Rong, B. Q. Chen, Z. Y. Zhu, and H. Q. Song, *Phys. Lett.* **B604**, 170 (2004).
 - [25] E.N.E. van Dalen, C. Fuchs, and A. Faessler, *Phys. Rev. Lett.* **95**, 022302 (2005).
 - [26] V. Baran, M. Colonna, V. Greco, and M. Di Toro, *Phys. Rep.* **410**, 335 (2005).
 - [27] W.-H. Long, N. Van Giai, and J. Meng, *Phys. Lett.* **B640**, 150 (2006).
 - [28] M. Dutra et al., *Phys. Rev. C* **85**, 035201 (2012).
 - [29] R. Chen, B.J. Cai, L.W. Chen, B.A. Li, X.H. Li, and C. Xu, *Phys. Rev. C* **85**, 024305 (2012).
 - [30] R. Sellahewa and A. Rios, *Phys. Rev. C* **90**, 054327 (2014).
 - [31] L. Ou, Z.X. Li, Y.X. Zhang, and M. Liu, *Phys. Lett.* **B697**, 246 (2011).
 - [32] S. Goriely, S. Hilaire, M. Girod, and S. Péru, *Phys. Rev. Lett.* **102**, 242501 (2009).
 - [33] C. Xu, B.A. Li, and L.W. Chen, *Phys. Rev. C* **82**, 054607 (2010).
 - [34] X.H. Li, W.J. Guo, B.A. Li, L.W. Chen, F.J. Fattoyev, and W.G. Newton, *Phys. Lett.* **B743**, 408 (2015).
 - [35] D.S. Coupland et al., arXiv:1406.4546
 - [36] H.Y. Kong, Y. Xia, J. Xu, L.W. Chen, B.A. Li, and Y.G. Ma, *Phys. Rev. C* **91**, 047601 (2015).
 - [37] A. Bohr and B. R. Mottelson, *Nuclear Structure*, Vols. I and II (W. A. Benjamin Inc., Reading, MA, 1975).
 - [38] O. Bohigas, A.M. Lane, and J. Martorell, *Phys. Rep.* **51**, 267 (1979).
 - [39] X. Roca-Maza et al., *Phys. Rev. C* **87**, 034301 (2013).
 - [40] J.-P. Blaizot, *Phys. Rep.* **64**, 171 (1980).
 - [41] P. Klüpfel, P.-G. Reinhard, T.J. Bürvenich, and J.A. Maruhn, *Phys. Rev. C* **79**, 034310 (2009).
 - [42] T. Lesinski, K. Bennaceur, T. Duguet, and J. Meyer, *Phys. Rev. C* **74**, 044315 (2006).
 - [43] E. Chabanat, P. Bonche, P. Haensel, J. Meyer, and R. Schaeffer, *Nucl. Phys.* **A627**, 710 (1997).
 - [44] S.S. Dietrich and B.L. Berman, *At. Data Nucl. Data Tables* **38**, 199 (1988).
 - [45] A. Tamii et al., *Phys. Rev. Lett.* **107**, 062502 (2011).
 - [46] P.-G. Reinhard and H. Flocard, *Nucl. Phys.* **A584**, 467 (1995).
 - [47] G. Colò, L.G. Cao, N. Van Giai, and L. Capelli, *Comput. Phys. Commun.* **184**, 142 (2013).
 - [48] M.N. Harakeh and A. van der Woude, *Giant Resonances-Fundamental High-frequency Modes of Nuclear Excitation* (Clarendon, Oxford, 2001).
 - [49] Z. Zhang and L.W. Chen, *Phys. Lett.* **B726**, 234 (2013).
 - [50] X. Roca-Maza, G. Colò, and H. Sagawa, *Phys. Rev. C* **86**, 031306(R) (2012).
 - [51] K. Yoshida and T. Nakatsukasa, *Phys. Rev. C* **88**, 034309 (2013).
 - [52] J.M. Pearson and S. Goriely, *Phys. Rev. C* **64**, 027301 (2001).
 - [53] L. Trippa, G. Colò, and E. Vigezzi, *Phys. Rev. C* **77**, 061304(R) (2008).
 - [54] B.A. Li and X. Han, *Phys. Lett.* **B727**, 276 (2013).